Journal Name

ARTICLE

Received 00th January 20xx,
Accepted 00th January 20xx

DOI: 10.1039/x0xx00000x

www.rsc.org/

Heterobimetallic Complexes of IrM (M = Fe^{II}, Co^{II}, and Ni^{II}) Core and Bridging 2-(Diphenylphosphino)pyridine: Electronic Structure and Electrochemical Behavior

Valeriy Cherepakhin,[a] Ashley Hellman,[a] Zhenzhuo Lan,[b] Shaama Mallikarjun Sharada,[a,b] and Travis J. Williams*[a]

Three complexes based on an Ir–M (M = Fe^{II}, Co^{II}, and Ni^{II}) heterobimetallic core and 2-(diphenylphosphino)pyridine (Ph_2PPy) ligand were synthesized via the reaction of *trans*-[IrCl(CO)($Ph_2PPy)_2$] and the corresponding metal chloride. Their structures were established by single-crystal X-ray diffraction as [Ir(CO)(μ-Cl)(μ-$Ph_2PPy)_2FeCl_2$]·$2CH_2Cl_2$ (**2**), [IrCl(CO)(μ-$Ph_2PPy)_2CoCl_2$]·$2CH_2Cl_2$ (**3**), and [Ir(CO)(μ-Cl)(μ-$Ph_2PPy)_2NiCl_2$]·$2CH_2Cl_2$ (**4**). Time-dependent DFT computations suggest a donor-acceptor interaction between a filled $5d_{z^2}$ orbital on iridium and an empty orbital on the first-row metal atom, which is supported by UV-vis studies. Magnetic moment measurements show that the first-row metals are in their high-spin electronic configurations. Cyclic voltammetry data show that all the complexes undergo irreversible decomposition upon either reduction or oxidation. Reduction of **4** proceeds through ECE mechanism. While these complexes are not stable to electrocatalysis conditions, the data presented here refine our understanding of the bonding synergies of the first-row and third-row metals.

Introduction

Homo- and heterodinuclear transition metal complexes are popular scaffolds for catalyst development.[1–3] Interest in such compounds is driven both by their complex electronic structures and unique catalytic activities, both made possible by synergy of the multiple metal centers. Particularly, activation of small molecules such as CO_2, isonitriles, alkenes, and alkynes by bimetallic complexes is a popular area in modern organometallic chemistry.[4,5] When in a chelate, 2-(diphenylphosphino)pyridine (Ph_2PPy) is a small-bite-angle ligand that, given the opportunity, prefers to serve as a bridge between two different metal atoms, thus facilitating M–M' bond formation. Homo- and heterodinuclear complexes bearing two bridging Ph_2PPy ligands are known since 1980,[6] and some iridium-containing complexes of this type are known: IrCu, IrTl, IrPd, IrHg,[7] IrCd,[8] and IrIr.[9]

Here we report the synthesis, spectroscopy, electrochemistry, and structural characterization of new heterodinuclear complexes based on Ir–Fe, Ir–Co, and Ir–Ni cores and bridging Ph_2PPy ligand. The rationale for bringing together the atoms of first- and third-row transition elements is their fundamentally different redox properties: we believe that combining one-electron processes available to the first row metals (e.g. Fe, Co, and Ni) and two-electron transitions that we have been studying on iridium[9] can enable new types of metal cluster catalysis.[10,11] Designing such reactivity begins with a detailed understanding of the synthesis and electronic structure of these heterobimetallics, which we report here.

Results and discussion

Synthesis and structure of the metal complexes

Dinuclear complexes **2** – **4** were obtained from the reactions of iridium precursor *trans*-[IrCl(CO)($Ph_2PPy)_2$] (**1**) and the corresponding dichlorometal etherate derivative, [$Fe_4Cl_8(THF)_6$], [$Co_4Cl_8(THF)_6$], or [$NiCl_2$(DME)] (DME = 1,2-dimethoxyethane), in dichloromethane at room temperature (Scheme 1). Compounds **2** – **4** crystallize from a dichloromethane solution as disolvates of orange (**2**), green (**3**), and red-pink (**4**) colors. The materials are soluble in dichloromethane and THF, but insoluble in benzene, toluene, ether, and hexane.

Scheme 1. Syntheses of complexes **2** – **4**.

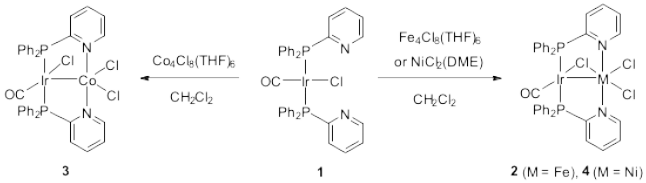

From cursory inspection of known Ph_2PPy-bridged Ir–M complexes, it appears that formation of the Ir–M bond can be achieved in two ways, according to the oxidation potential of the M atom. When M has low positive oxidation potential (Cu^{I}, Tl^{I}, Pb^{II},[12] Cd^{II}), iridium-metal bond appears to result from a donor-acceptor interaction between the filled $5d_{z^2}$ orbital on iridium and a corresponding empty orbital on M atom. In this type of complex, iridium atom adopts a distorted square pyramidal geometry. When the metal has a high positive oxidation potential (Pd^{II} and Hg^{II}), it facilitates the oxidative addition of an M–X bond to iridium atom, resulting in Ir–M bond formation and the octahedral geometry of the Ir^{III} atom. We find that Fe^{II}, Co^{II}, and Ni^{II} conform to the former pattern, and we observe complexes **2** – **4** to have an $Ir^{I}\rightarrow M^{II}$ type of interaction, which was subsequently confirmed by X-ray crystallography.

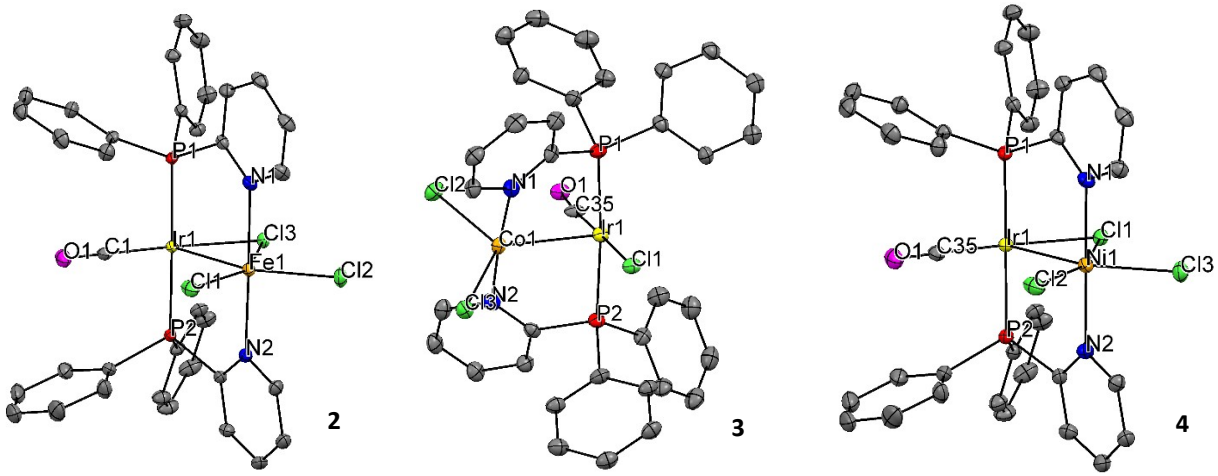

Figure 1. Molecular structures of **2**, **3**, and **4** shown with 50% probability ellipsoids. Hydrogen atoms and dichloromethane molecules are omitted for clarity. Selected bond distances (Å): (**2**) Ir1–Fe1 2.7659(7), (**3**) Ir1–Co1 2.596(6), and (**4**) Ir1–Ni1 2.7022(13).

The structures of **2** – **4** were established by single-crystal X-ray diffraction (Figure 1). The complexes possess dinuclear structure enabled by the bridging Ph_2PPy ligand. Intermetallic distances in **2** – **4** (Ir1–Fe1 2.7659(7), Ir1–Co1 2.596(6), and Ir1–Ni1 2.7022(13) Å) are shorter than the sum of van der Waals radii of iridium and the first-row metals which is 3.78 Å, indicating a significant intermetallic interaction. Moreover, complex **3** exhibits the shortest Ir–M distance in the series indicating high covalency of the Ir–Co bond. The overall metal-ligand arrangement is consistent with Ir^{I} and M^{II} interaction where iridium atom acts as an L-type ligand for M^{II}

atoms. Complexes **2** and **4** are isomorphous with the distorted octahedral coordination geometries of Fe^{II} and Ni^{II} atoms. The equatorial bond angles range from 54 to 118° in these compounds: Cl1–Fe1–Cl2 117.70(3), Cl1–Fe1–Ir1 96.17(3), Cl2–Fe1–Cl3 93.56(2), Cl3–Fe1–Ir1 52.574(19); Cl2–Ni1–Cl3 110.89(6), Cl2–Ni1–Ir1 101.12(5), Cl3–Ni1–Cl1 93.79(5), and Cl1–Ni1–Ir1 54.21(3). The Ir–M bonds in these compounds are stabilized by the bridging chloride ligands.

Surprisingly, the structure of complex **3** deviates from **2** and **4**: the torsion angle P1–Ir1–Co1–N1 is significantly larger compared to the other analogs (28.30 vs. 1.62 (**2**) and 1.49° (**4**)), resulting in the absence of the bridging chloride ligand, and enabling a distorted trigonal bipyramidal geometry of Co^{II} atom with the equatorial bond angles ranging from 113 to 125°: Cl3–Co1–Ir1 124.79(14), Cl2–Co1–Ir1 122.58(16), and Cl2–Co1–Cl3 112.63(19)°. The absence of bridging chloride in complex **3** is also confirmed by geometry relaxation calculations carried out using density functional theory.

Complex **4** represents a rare example of Ir–Ni bond, the other cases are limited to $[IrNi_8(CO)_{18}]^{3-}$ (2.015 – 3.047 Å)[13] and $[(Cp^*IrS)_4Ni]^{2+/+}$ (2.596 – 2.699 Å).[14]

Spectroscopic studies

Complexes **2** – **4** were studied by ^1H NMR spectroscopy. The proton spectra exhibit broad peaks consistent with the presence of paramagnetic Fe^{II}, Co^{II}, and Ni^{II} atoms. Effective magnetic moments (μ_{eff}) of **2** – **4** were measured by Evans method using CH_2Cl_2 peaks in ^1H NMR spectra (Table 1).[15] Complex **4** has μ_{eff} = 2.86 BM, which agrees with the spin-only magnetic moment value (μ_{so} = 2.83 BM) for an octahedral high-spin ion with d^8-configuration ($^3A_2$ ground state of Ni^{II}). Effective magnetic moments of **2** and **3**, however, deviate from the expected spin-only values: μ_{eff}(**2**) = 5.04 BM (μ_{so} = 4.90 BM) and μ_{eff}(**3**) = 5.04 BM (μ_{so} = 3.87 BM). We attribute this deviation to significant orbital contribution to the magnetic moments, which is expected for $^5T_2$ and $^4T_1$ ground states of Fe^{II} and Co^{II} respectively. Thus, in all the complexes the first-row metal atoms exist in their high-spin configurations, and the Ir–M interaction does not cause high-spin to low-spin transition at room temperature in a dichloromethane solution.

Table 1. Summarized spectroscopic data.

Compound	ν(CO), cm^{-1}	μ_{eff}, BM	λ_{max}, nm
1	1959	0	340, 387, 440
2	2008	5.04	343, 438
3	2012	5.04	330[a], 361[a], 442
4	2010	2.86	330[a], 374, 513

[a] Shoulder

IR spectroscopy demonstrates that ν(CO) vibration is sensitive to the presence of Ir–M bond in **2** – **4**. The corresponding absorption band in the dinuclear complexes appears at 2008 – 2012 cm^{-1}, whereas **1** has the band at 1959 cm^{-1}. The observation indicates that Ir–M interaction reduces electron density on the iridium atom and, consequently, decreases back donation to the CO ligand. This effect was detected previously in iridium and iron heterodinuclear complexes: $[IrI(CO)_2(\mu\text{-}Ph_2PPy)_2CdI_2]$ (2002, 2066 cm^{-1}),[8] $[IrCl(CO)(\mu\text{-}Ph_2PPy)_2Cu]BF_4$ (1983 cm^{-1}), $[IrCl(CO)(\mu\text{-}Ph_2PPy)_2Tl]PF_6$ (1994 cm^{-1}),[7] and $[(OC)_3Fe(\mu\text{-}Ph_2PPy)ML_n]$.[16]

Complexes **2** – **4** were investigated by electronic absorption spectroscopy in dichloromethane solution at room temperature (Figure 2). According to Kuang *et al.*,[8] complex **1** has absorption bands at 338, 386, and 440 nm, that is the three-band pattern typical for Vaska-type complexes.[17] Installation of the second metal atom seems to have a minor effect on the number and intensity of the absorption bands in the resulting spectrum. Thus, the spectra of **1** – **4** are quite similar having one or two strong bands with λ_{max} < 400 nm (ε = 3700 – 5200 $M^{-1}\,cm^{-1}$) and a weak band with λ_{max} > 400 nm (ε = 400 – 1400 $M^{-1}\,cm^{-1}$). An analogous picture is observed in the case of $[IrX(CO)(\mu\text{-}PN)_2ML_n]$ (X = Cl – I, M = Na, K, Tl, Sn, Pb).[12,18] The lowest energy band of complex **4** demonstrates a significant bathochromic shift (513 nm) compared to the same band of **1** – **3** (437 – 442 nm).

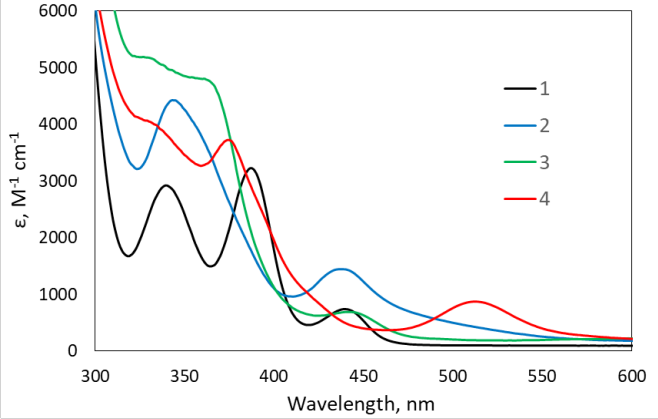

Figure 2. Electronic absorption spectra of **1** – **4** in CH_2Cl_2 at 25 °C.

Computational studies

Although the electronic absorption spectra of Vaska-type complexes and the complexes with Ir–M bonds had been discussed before, the assignment of the bands made by different authors is contradictory. Therefore, we performed a computational study to assign the high-energy bands at 330 – 340 nm using time-dependent density functional theory.[19] We found that complexes **1** – **4** are challenging systems for theoretical analysis because of high sensitivity of peak locations to the choice of effective core potentials for transition metal atoms. Extreme caution is advised with interpretation of computational UV-Vis spectra, for this reason we restricted our theoretical analysis to characterizing the origins of transitions reflected in the UV-Vis spectra using natural transition orbitals (NTOs).[20]

Table 2 illustrates NTO hole-particle pairs related to the two largest excitation amplitudes in complexes **1** – **4**, and table 3 shows the assignment of the corresponding experimental absorption bands. In complex **1**, the observed band at 340 nm is assigned to the apparent metal-to-ligand charge transfer (MLCT) from occupied $5d_{z^2}$ orbital of the iridium center to an empty π* orbital of the carbonyl ligand (E_{calc} = 3.62 eV). The second NTO pair originates from MLCT between the filled d_{xz}/d_{yz} orbital of iridium atom and an

antibonding orbital which is delocalized among all four coordinating atoms (E_{calc} = 4.20 eV, 295 nm). This latter transition seems to appear near the absorption edge of the solution.

Table 2. The dominant natural transition orbital pairs for the excited states corresponding to the largest oscillator strength for **1** – **4**.

Compound	Hole → Particle(1)	Hole → Particle(2)
1	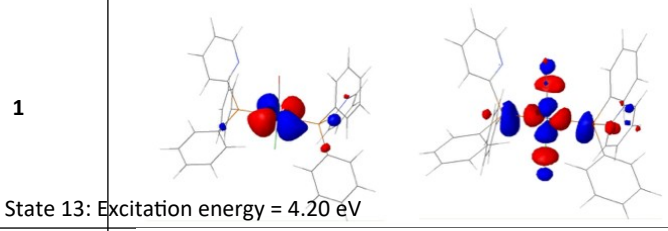 State 13: Excitation energy = 4.20 eV	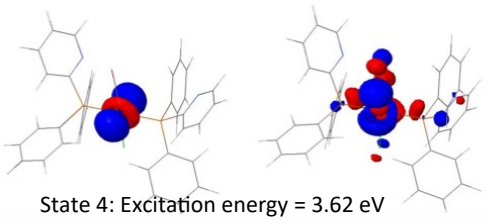 State 4: Excitation energy = 3.62 eV
2	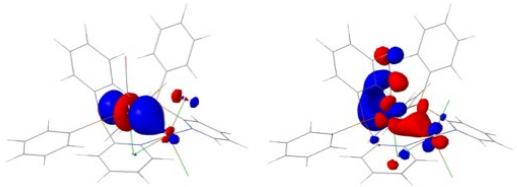 State 8-β: Excitation energy = 3.76 eV	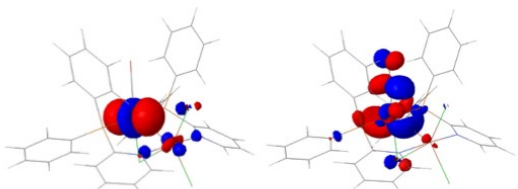 State 8-α: Excitation energy = 3.76 eV
3	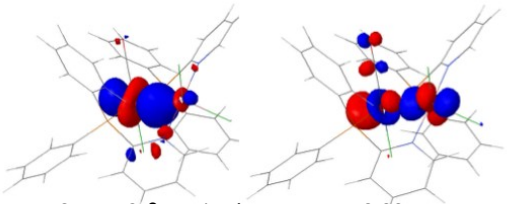 State 12-β: Excitation energy = 3.99 eV	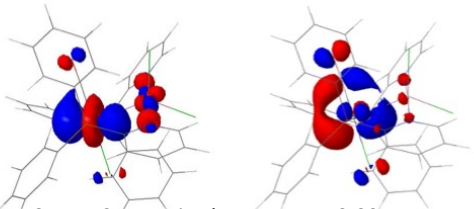 State 12-α: Excitation energy = 3.99 eV
4	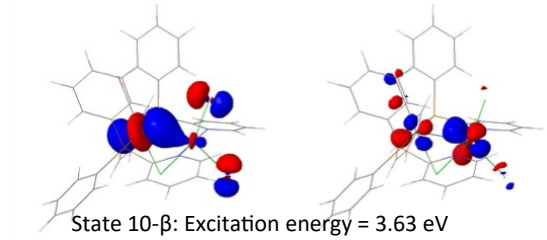 State 10-β: Excitation energy = 3.63 eV	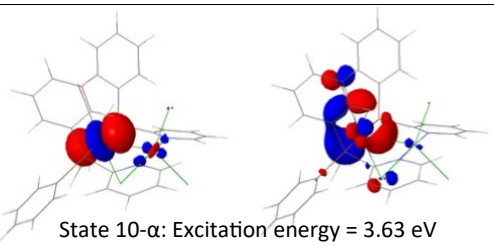 State 10-α: Excitation energy = 3.63 eV

Table 3. Assignment of the experimental UV-Vis absorption bands.

Com-pound	λ_{max}, nm	*E* (exp.), eV	*E* (calc.), eV	Assignment
1	340 387 440	3.65 3.20 2.82	4.20 3.62	MLCT MLCT
2	343 438	3.62 2.83	3.76	MLCT (α), IC (β)
3	330 361 442	3.76 3.43 2.81	3.99	MLCT (α), IC (β)
4	330 374 513	3.76 3.32 2.42	3.63	MLCT (α), IC (β)

Analysis of alpha spin-orbitals demonstrates that the NTO pairs in the series **2** – **4** are very similar in shape and correspond to the MLCT from $5d_{z^2}$ orbital of iridium atom to the carbonyl ligand, the same as in complex **1** (Table 2, right column). While the orbitals of iron and nickel do not contribute significantly to the ground states in this series of NTOs, the orbitals of cobalt do, which could be the reason for the deviating crystal structure of **3** and the shortest distance Ir–Co in the series.

Although NTOs derived from beta spin-orbitals of compounds **2** – **4** have a complex shape, we describe these as intra-cluster (IC) transitions, since the electron density of the ground and exited states is delocalized between both metal atoms in Ir–M cluster (Table 2, left column). Moreover, complex **4** exhibits significant contribution of *p*-orbitals of terminal chloride ligands to the ground state, which is not observed in **1** – **3** (state 10-β).

To sum up, the computational data suggest that the observed UV-Vis absorption bands in the range 330 – 340 nm result from the electronic transitions from molecular orbitals with a high contribution of $5d_{z^2}$ orbital of iridium atom. The transitions can be described as a combination of IC and MLCTs.

Electrochemical studies

Electrochemical properties of compounds **2** – **4** were assessed by cyclic voltammetry in 0.1 M solution of $[Bu_4N][PF_6]$ in dichloromethane and tetrahydrofuran at room temperature under

nitrogen atmosphere. None of the complexes showed an electrochemically reversible redox event upon either oxidation or reduction. Moreover, in most cases the products of electrochemical reactions deposited on the electrode surface, except for reduction of complex **4** and oxidation of complex **3**.

Upon scanning cathodically in dichloromethane, complex **4** undergoes reduction at E_p = –1.49 V (25 mV/s, vs. $Fc^{+/0}$). At slow scan rates (25 and 50 mV/s), the reduction event is chemically irreversible, with no return oxidation wave (Figure 3). As the scan rate is increased, the return oxidation wave appears at –0.88 V (1000 mV/s, ΔE_p = 740 mV, vs. $Fc^{+/0}$). suggesting an ECE mechanism for the transformation of **4**.[21] The increase of the scan rate also causes higher peak currents for both the anodic and cathodic waves along with the wave shift to more positive and negative potentials, respectively. Plotting log(peak current) *vs.* log(scan rate) yields a linear relationship with a slope of approximately 0.5, indicating that redox couples involved in the ECE mechanism obey the Randles–Sevcik equation, and that freely diffusing molecular species are contributing to the observed electrochemical event rather than species adsorbed on the electrode surface (Figure S12). Additionally, plotting peak current *vs.* the square root of the scan rate yields a linear relationship, which is also consistent with freely diffusing complex **4** and its reduced forms (Figure S13).

Applying positive potential in tetrahydrofuran, complex **3** undergoes two chemically irreversible oxidation events at E_p = 0.43 and 1.05 V (at 25 mV/s) without any sign of return reduction (Figure 3). Increasing the scan rate up to 2000 mV/s does not result in the appearance of the return reduction waves, which is the evidence for a fast chemical reaction that follows the oxidation steps.

Overall, the absence of well-behaved electrochemically reversible redox couples involving complexes **2** – **4** indicates high reactivity of their reduced and oxidized forms that are not stable under the experiment conditions.

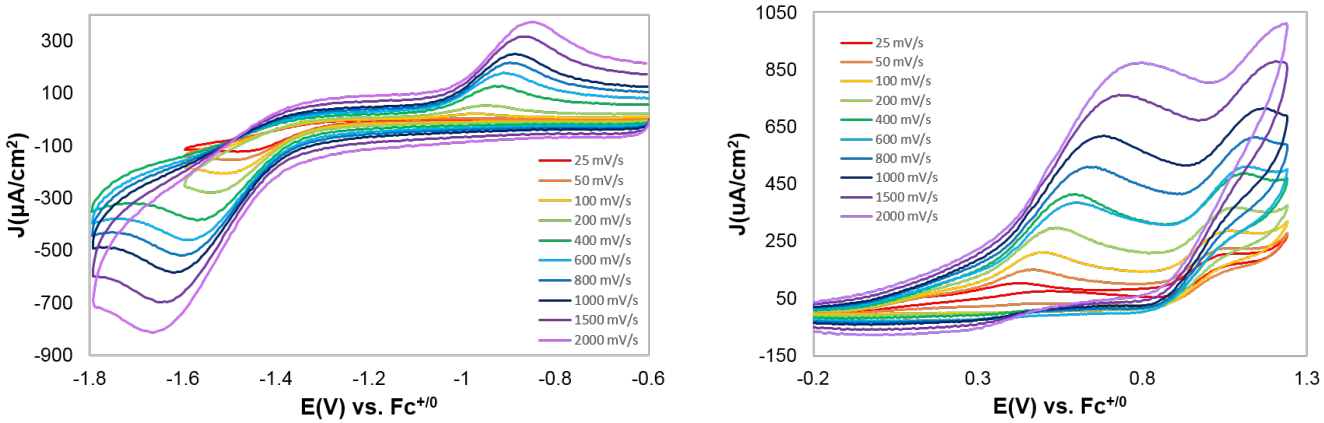

Figure 3. Cyclic voltammograms of 1 mM **4** in CH_2Cl_2 (left) and 1 mM **3** in THF (right) with 0.1 M $[Bu_4N][PF_6]$ at various scan rates.

Experimental section

Materials and methods

$[Fe_4Cl_8(THF)_6]$ and $[Co_4Cl_8(THF)_6]$ were synthesized according to the described procedures.[22,23] $[NiCl_2(DME)]$, $[Ir_2Cl_2(COD)_2]$, 2-(Diphenylphosphino)pyridine, and carbon monoxide were purchased from commercial sources and used without further purification. Dichloromethane, diethyl ether, and hexane were dried according to standard methods. Dichloromethane-d_2 was purchased from Cambridge Isotopes Laboratories and dried over CaH_2 followed by distillation. All the synthetic procedures were carried out in a Vacuum Atmosphere glove box under nitrogen (1 – 10 ppm O_2). ^1H, ^{13}C, and ^{31}P NMR spectra were recorded on Varian VNMRS 500 and 600 spectrometers, and processed using MestReNova v11.0.2. All chemical shifts are reported in ppm and referenced to the residual ^1H or ^{13}C solvent peaks. NMR spectra of air-sensitive compounds were taken in 8" J. Young tubes (Wilmad or Norell) with Teflon valve plugs. Infrared spectra were recorded on Bruker OPUS FTIR spectrometer. MALDI-MS spectra were acquired on Bruker Autoflex Speed MALDI Mass Spectrometer.

Elemental analyses were conducted on Flash 2000 CHNS Elemental Analyzer. UV-Vis spectra were recorded on Perkin-Elmer UV/Vis/NIR spectrophotometer.

Electrochemistry experiments were carried out using a Pine potentiostat. The experiments were performed in a single compartment electrochemical cell under nitrogen atmosphere using a 3 mm diameter glassy carbon electrode as the working electrode, a platinum wire as auxiliary electrode and a silver wire as the reference electrode. All experiments were referenced relative to ferrocene (Fc) with the $Fc^{+/0}$ couple at 0.0 V using decamethylferrocene as an internal standard. All experiments were performed with 0.1 M tetrabutylammonium hexafluorophosphate as a supporting electrolyte.

***trans*-[IrCl(CO)(Ph_2PPy)$_2$] (1).** This compound was synthesized from $[Ir_2Cl_2(COD)_2]$, Ph_2PPy, and CO in CH_2Cl_2 according to the described procedure.[7,8,24] ^1H NMR (600 MHz, CD_2Cl_2): δ 8.75 (ddd, *J* = 4.7, 1.8, 1.0 Hz, 1H), 8.03 (d, *J* = 7.8 Hz, 1H), 7.90 – 7.80 (m, 4H), 7.73 (td, *J* = 7.7, 1.7 Hz, 1H), 7.49 – 7.39 (m, 6H), 7.30 (ddd, *J* = 7.7, 4.7, 1.1 Hz, 1H). $^{13}C\{^1H\}$ NMR (151 MHz, CD_2Cl_2): δ 171.17, 157.63 (t, *J* = 36.9 Hz), 150.40, 135.86, 135.61, 132.40 (t, *J* = 27.2 Hz), 131.92 (t, *J* = 11.8 Hz), 130.87, 128.40, 124.52. $^{31}P\{^1H\}$ NMR (243 MHz,

CD_2Cl_2): δ 24.37. IR (KBr, cm^{-1}): ν(CO) 1959. MALDI-MS: *m/z* [M – CO]$^+$ calcd. 754.10, found 753.96; [M – COCl]$^+$ calcd. 719.14, found 718.97.

General procedure for the synthesis of 2 and 3. In a glovebox, **1** (20 mg, 2.56 x 10^{-5} mol) and [$M_4Cl_8(THF)_6$] (6 mg, 6.39 x 10^{-6} mol) were mixed with dry CH_2Cl_2 (5 mL) and stirred at room temperature for 5 h. The resulting solution was filtered and concentrated to ca. 1 mL in vacuum. Slow addition of diethyl ether afforded crystallization of the product. It was filtered, washed with ether, and dried in vacuum.

[Ir(CO)(μ-Cl)(μ-$Ph_2PPy)_2FeCl_2$]·$2CH_2Cl_2$ (2). Orange crystalline powder (20 mg, 72%). Crystals suitable for X-ray analysis were obtained by slow addition of diethyl ether to CH_2Cl_2 solution. ^{1}H NMR (500 MHz, CD_2Cl_2): δ 6.50 – 10.00 (m, ArH). $^{31}P\{^1H\}$ NMR (202 MHz, CD_2Cl_2): δ 3.03. IR (KBr, cm^{-1}): ν(CO) 2009, 1968. MALDI-MS: *m/z* [M – COCl]$^+$ calcd. 845.01, found 844.84. Anal. calcd for $C_{37}H_{32}Cl_7FeIrN_2OP_2$: C 41.19, H 2.99, N 2.60. Found: C 41.56, H 3.15, N 3.09.

[IrCl(CO)(μ-$Ph_2PPy)_2CoCl_2$]·$2CH_2Cl_2$ (3). Green crystalline powder (15 mg, 54%). Crystals suitable for X-ray analysis were obtained by slow addition of diethyl ether to CH_2Cl_2 solution. ^{1}H NMR (600 MHz, CD_2Cl_2): δ 10.02 (br s), 9.28 (br s), 8.10 (br s), 2.65 (br s). IR (KBr, cm^{-1}): ν(CO) 2010, 1968. MALDI-MS: *m/z* [M – Cl]$^+$ calcd. 876.00, found 875.94; [M – COCl]$^+$ calcd. 848.01, found 848.02. Anal. calcd for $C_{37}H_{32}Cl_7CoIrN_2OP_2$: C 41.08, H 2.98, N 2.59. Found: C 41.12, H 3.10, N 2.70.

[Ir(CO)(μ-Cl)(μ-$Ph_2PPy)_2NiCl_2$]·$2CH_2Cl_2$ (4). In a glovebox, **1** (100 mg, 0.128 mmol) and [$NiCl_2$(DME)] (28 mg, 0.128 mmol) were mixed with dry CH_2Cl_2 (5 mL) and stirred at room temperature overnight. The dark-pink suspension was concentrated to ca. 2 mL and the resulting precipitate was filtered, washed with minimal amount of CH_2Cl_2, and dried in vacuum. The compound was obtained as a pink powder (103 mg, 75%). Crystals suitable for X-ray analysis were obtained by slow evaporation of CH_2Cl_2 solution. ^{1}H NMR (500 MHz, CD_2Cl_2): δ 5.80 – 6.90 (m, ArH). $^{31}P\{^1H\}$ NMR (202 MHz, CD_2Cl_2): δ 24.42. IR (KBr, cm^{-1}): ν(CO) 2016, 2010, 1967. MALDI-MS: *m/z* [M – Cl]$^+$ calcd. 875.00, found 875.07; [M – COCl]$^+$ calcd. 847.01, found 847.05. Anal. calcd for $C_{37}H_{32}Cl_7IrN_2NiOP_2$: C 41.08, H 2.98, N 2.59. Found: C 40.80, H 3.12, N 2.89.

Computational methods

All simulations are carried out using the ab initio quantum chemistry software, Q-Chem 5.1.2.[25] Geometry optimizations and excited state calculations are carried out using the CAM-B3LYP functional[26] along with the LANL08[27] effective core potential (ECP) for Ir, Ni, Fe, and Co, the 6-311G* basis set for N, P, and Cl, and 6-31G* basis set for H, C, and O atoms. The choice of level of theory is guided by previous work with Pt complexes by Roy and coworkers.[28] NTOs are visualized using Jmol.[29]

Conclusions

We reported a synthesis and crystal structures of a series of pyridyl-phosphine complexes **2** – **4** containing Ir–Fe, Ir–Co, and Ir–Ni heterobimetallic cores. The electronic structure of these compounds was studied by spectroscopic (NMR, IR, and UV-Vis) and computational (time-dependent DFT) methods to get an insight to the nature of iridium-metal bonding. The typical high-spin electronic states of Fe^{II}, Co^{II}, and Ni^{II} atoms are not affected by the coordination with Ir^{I}. Computational data suggest that the observed UV-Vis absorption bands result from the electronic transitions from molecular orbitals that have a dominant contribution of $5d_{z^2}$ orbital of iridium atom. Electrochemical studies showed that the oxidized and reduced forms of **2** – **4** are highly reactive and decompose under the experiment conditions, which demonstrates poor ability of iridium(I) to stabilize the first-row transition metals in their potential application in electrocatalysis.

Conflicts of interest

There are no conflicts to declare.

Acknowledgements

This work is sponsored by the NSF (CHE-1856395), and the Hydrocarbon Research Foundation. We thank the NSF (DBI-0821671, CHE-0840366, and CHE-1048807) and NIH (1 S10 RR25432) for sponsorship of research instrumentation. V.C. acknowledges Sonosky fellowship support from the USC Wrigley Institute for Environmental Studies. We thank Prof. Ralf Haiges for help with X-ray crystallography. We are grateful to Prof. Smaranda C. Marinescu (NSF CHE-1555387) for discussions and use of instrumentation. S.M.S. acknowledges University of Southern California's startup funds and High-Performance Computing resources for supporting this work. Z.L.'s work is supported by the Graduate Fellowship and TLARGI fellowship from USC.

Notes and references

1 D. W. Stephan, *Coord. Chem. Rev.*, **1989**, 95, 41–107;
2 S. Komiya, *Coord. Chem. Rev.*, **2012**, 256, 556–573;
3 B. G. Cooper, J. W. Napoline, C. M. Thomas, *Catalysis Reviews: Science and Engineering*, **2012**, 54, 1–40;
4 M. Knorr, I. Jourdain, *Coord. Chem. Rev.*, **2017**, 350, 217–247;
5 J. Blanco-Urgoiti, L. Añorbe, L. Pérez-Serrano, G. Domínguеza, J. Pérez-Castells, *Chem. Soc. Rev.*, **2004**, 33, 32–42;
6 J. P. Farr, M. M. Olmstead, A. L. Balch, *J. Am. Chem. Soc.*, **1980**, 102, 6654–6656;
7 G. Francio, R. Scopelliti, C. G. Arena, G. Bruno, D. Drommi, F. Faraone, *Organometallics*, **1998**, 17, 338–347;
8 S.-M. Kuang, F. Xue, Z.-Z. Zhang, W.-M. Xue, C.-M. Che, T. C. W. Mak, *J. Chem. Soc., Dalton Trans.*, **1997**, 3409–3410;
9 9a. S.-M. Kuang, F. Xue, T. C. W. Mak, Z.-Z. Zhang, *Inorg. Chim. Acta*, **1999**, 284, 119–123; 9b. Z. Lu, V. Cherepakhin, I. Demianets, P. J. Lauridsen, T. J. Williams, *Chem. Commun.*, **2018**, 54, 7711–7724; 9c. V. Cherepakhin, T. J. Williams, *ACS Catal.*, **2018**, 8, 3754–3763;
10 K. D. Wells, M. J. Ferguson, R. McDonald, M. Cowie, *Organometallics*, **2008**, 27, 691–703;

11 J. M. López-Valbuena, E. C. Escudero-Adan, J. Benet-Buchholz, Z. Freixa, P. W. N. M. van Leeuwen, *Dalton Trans.*, **2010**, 39, 8560–8574;
12 A. L. Balch, F. Neve, M. M. Olmstead, *Inorg. Chem.*, **1991**, 30, 3395–3402;
13 A. Ceriotti, R. D. Pergola, L. Garlaschelli, M. Manassero, N. Masciocchi, M. Sansoni, *J. Chem. Soc., Dalton Trans.*, **1991**, 2357–2362;
14 Z. Tang, Y. Nomura, S. Kuwata, Y. Ishii, Y. Mizobe, M. Hidai, *Inorg. Chem.*, **1998**, 37, 4909–4920;
15 D. F. Evans, *J. Chem. Soc.*, **1959**, 2003–2005; J. L. Deutsch, S. M. Poling, *J. Chem. Educ.*, **1969**, 46, 167–168;
16 Z.-Z. Zhang, H. Cheng, S.-M. Kuang, Y.-Q. Zhou, Z.-X. Liu, J.-K. Zhang, H.-G. Wang, *J. Organomet. Chem.*, **1996**, 516, 1–10; S.-L. Li, T. C. W. Mak, Z.-Z. Zhang, *J. Chem. Soc., Dalton Trans.*, **1996**, 3475–3483;
17 R. Brady, B. R. Flynn, G. L. Goeffroy, H. B. Gray, J. Peone, L. Vaska, *Inorg. Chem.*, **1976**, 15, 1485–1488;
18 A. L. Balch, F. Neve, M. M. Olmstead, *J. Am. Chem. Soc.*, **1991**, 113, 2995–3001;
19 D. Andreas, M. Head-Gordon, *Chem. Rev.*, **2005**, 4009–4037;
20 20a. L. M. Richard, *J. Chem. Phys.*, **2003**, 118, 4775-4777; 20b. A. Ipatov, F. Cordova, L. J. Doriol, M. E. Casida. *J. Mol. Struct.: THEOCHEM*, **2009**, 914, 60–73; 20c. M. Kaupp, M. Renz, M. Parthey, M. Stolte, F. Wurthner, C. Lambert, *Phys. Chem. Chem. Phys.,* **2011**, 13, 16973–16986;
21 N. Elgrishi, K. J. Rountree, B. D. Mccarthy, E. S. Rountree, T. T. Eisenhart, J. L. Dempsey, *J. Chem. Educ.*, **2018**, 95, 197–206;
22 F. A. Cotton, R. L. Luck, K.-A. Son, *Inorg. Chim. Acta*, **1991**, 179, 11–15;
23 P. Sobota, Z. Olejnik, J. Utko, T. Lis, *Polyhedron*, **1993**, 12, 613–616;
24 M. J. Burk, R. H. Crabtree, *Inorg. Chem.*, **1986**, 25, 931–932;
25 Y. Shao, Z. Gan, E. Epifanovsky, E., et al., *Mol. Phys.*, **2015**, 113, 184–215;
26 Y. Takeshi, D. P. Tew, N. C. Handy., *Chem. Phys. Lett.,* **2004**, 393, 51–57;
27 L. E. Roy, P. J. Hay, R. L. Martin., *J. Chem. Theory Comput.*, **2008**, 4, 1029–1031;
28 L. E. Roy, G. Scalmani, R. Kobayashi, E. R. Batista, *Dalton Trans.*, **2009**, 34, 6719–6721;
29 Jmol: an open-source Java viewer for chemical structures in 3D (http://www.jmol.org/).